UNIVERSITÄT AUGSBURG
Universitätsbibliothek

OPEN ACCESS
OPUS AUGSBURG

Regnase-1 overexpression as a therapeutic approach of Marfan syndrome

Marie Noormalal, Nesrin Schmiedel, Tarik Bozoglu, Andrea Matzen, Susanne Hille, Dima Ibrahim Basha, Prithviraj Manohar Vijaya Shetty, Anja Wolf, Marcin Zaradzki, Rawa Arif, Thomas Pühler, Georg Lutter, Andreas H. Wagner, Christian Kupatt, Derk Frank, Norbert Frey, Anca Remes, Oliver J. Müller

Angaben zur Veröffentlichung / Publication details:

Noormalal, Marie, Nesrin Schmiedel, Tarik Bozoglu, Andrea Matzen, Susanne Hille, Dima Ibrahim Basha, Prithviraj Manohar Vijaya Shetty, et al. 2024. "Regnase-1 overexpression as a therapeutic approach of Marfan syndrome." *Molecular Therapy: Methods & Clinical Development* 32 (1): 101163. https://doi.org/10.1016/j.omtm.2023.101163.

Nutzungsbedingungen / Terms of use: **CC BY-NC-ND 4.0**

Dieses Dokument wird unter folgenden Bedingungen zur Verfügung gestellt: / This document is made available under these conditions:
CC-BY-NC-ND 4.0: Creative Commons: Namensnennung - Nicht kommerziell - Keine Bearbeitung
Weitere Informationen finden Sie unter: / For more information see:
https://creativecommons.org/licenses/by-nc-nd/4.0/deed.de

Molecular Therapy
Methods & Clinical Development
Original Article

Regnase-1 overexpression as a therapeutic approach of Marfan syndrome

Marie Noormalal,[1] Nesrin Schmiedel,[1] Tarik Bozoglu,[2] Andrea Matzen,[1] Susanne Hille,[1] Dima Ibrahim Basha,[1] Prithviraj Manohar Vijaya Shetty,[1] Anja Wolf,[2] Marcin Zaradzki,[3] Rawa Arif,[3] Thomas Pühler,[4] Georg Lutter,[4] Andreas H. Wagner,[5] Christian Kupatt,[2] Derk Frank,[1] Norbert Frey,[6] Anca Remes,[1] and Oliver J. Müller[1]

[1]Department of Internal Medicine III, University of Kiel, and German Centre for Cardiovascular Research, Partner Site Hamburg/Kiel/Lübeck, Kiel, Germany; [2]Department of Internal Medicine I, Klinikum rechts der Isar, Munich, and German Centre for Cardiovascular Research, Partner Site Munich, Munich, Germany; [3]Department of Cardiac Surgery, University Hospital Heidelberg, Heidelberg, and German Centre for Cardiovascular Research, Partner Site Heidelberg/Mannheim, Heidelberg, Germany; [4]Department of Cardiac and Vascular Surgery, University of Kiel and University Hospital Schleswig-Holstein, Kiel, and German Centre for Cardiovascular Research, Partner Site Hamburg/Kiel/Lübeck, Kiel, Germany; [5]Department of Cardiovascular Physiology, Heidelberg University, Heidelberg, Germany; [6]Department of Internal Medicine III, University Hospital Heidelberg, and German Centre for Cardiovascular Research, Partner Site Heidelberg/Mannheim, Heidelberg, Germany

Rupture or dissection of thoracic aortic aneurysms is still the leading cause of death for patients diagnosed with Marfan syndrome. Inflammation and matrix digestion regulated by matrix metalloproteases (MMPs) play a major role in the pathological remodeling of the aortic media. Regnase-1 is an endoribonuclease shown to cleave the mRNA of proinflammatory cytokines, such as interleukin-6. Considering the major anti-inflammatory effects of regnase-1, here, we aimed to determine whether adeno-associated virus (AAV)–mediated vascular overexpression of the protein could provide protection from the development and progression of aortic aneurysms in Marfan syndrome. The overexpression of regnase-1 resulted in a marked decrease in inflammatory parameters and elastin degradation in aortic smooth muscle cells *in vitro*. Intravenous injection of a vascular-targeted AAV vector resulted in the efficient transduction of the aortic wall and overexpression of regnase-1 in a murine model of Marfan syndrome, associated with lower circulating levels of proinflammatory cytokines and decreased MMP expression and activity. Regnase-1 overexpression strongly improved elastin architecture in the media and reduced aortic diameter at distinct locations. Therefore, AAV-mediated regnase-1 overexpression may represent a novel gene therapy approach for inhibiting aortic aneurysms in Marfan syndrome.

INTRODUCTION

Marfan syndrome is a rare autosomal-dominant genetic disease caused by loss-of-function mutations in the gene encoding fibrillin-1, resulting in structural changes in microfibrils and elastic fibers in large arteries and other organs such as eyes and the skeletal system.[1] Cardiovascular complications comprise the formation of aortic aneurysms with a high risk of rupture or dissection, representing the main mortality risk for affected patients.[2]

It was previously shown that plasma levels of transforming growth factor β (TGF-β) increase in Marfan patients and the fibrillin-1 hypomorphic mgR/mgR murine model of Marfan syndrome.[3] TGF-β is known to enhance the activation and secretion of matrix metalloproteases (MMPs), which digest matrix components such as elastin, gelatin, and collagen, and decrease the stability of the aortic wall.[4] In addition to the elastolytic activity, it is known that MMP2 and MMP9 have adverse effects on vascular smooth muscle cells (SMCs) in thoracic aneurysms in mgR/mgR mice, presenting as apoptosis and decreased contractility.[5] Nonspecific MMP inhibition by doxycycline is known to have beneficial effects on aortic dilatation in Marfan syndrome.[6]

The inflammatory component plays a central role in the pathogenesis of the disease, including the formation of aortic aneurysms. Plasma levels of proinflammatory cytokines such as monocyte chemoattractant protein-1 (MCP-1) and, more important, interleukin-6 (IL-6) were demonstrated to be higher in Marfan patients[7] and in mgR/mgR mice[8] compared to controls. Consistently, it was shown that IL-6 deficiency causes less extracellular matrix degeneration in mgR/mgR mice.[8] Elevated levels of cytokines also lead to the infiltration of immune cells throughout the media,[7] complementing the factors that lead to increased vessel fragility in Marfan patients.

Regnase-1 is a newly identified endoribonuclease that cleaves the mRNA of targets such as IL-6, IL-12, and IL-8.[9,10] Thus, their stability and expression are decreased, indicating an anti-inflammatory effect. In addition, regnase-1 was shown to act as a negative regulator of

Received 31 May 2023; accepted 16 November 2023;
https://doi.org/10.1016/j.omtm.2023.101163.

Correspondence: Anca Remes, University Hospital Schleswig Holstein, Arnold-Heller-Str. 3, 24105 Kiel, Germany.
E-mail: anca.remes@uksh.de
Correspondence: Oliver Müller, University Hospital Schleswig Holstein, Arnold-Heller-Str. 3, 24105 Kiel, Germany.
E-mail: oliver.mueller@uksh.de

This is an open access article under the CC BY-NC-ND license (http://creativecommons.org/licenses/by-nc-nd/4.0/).

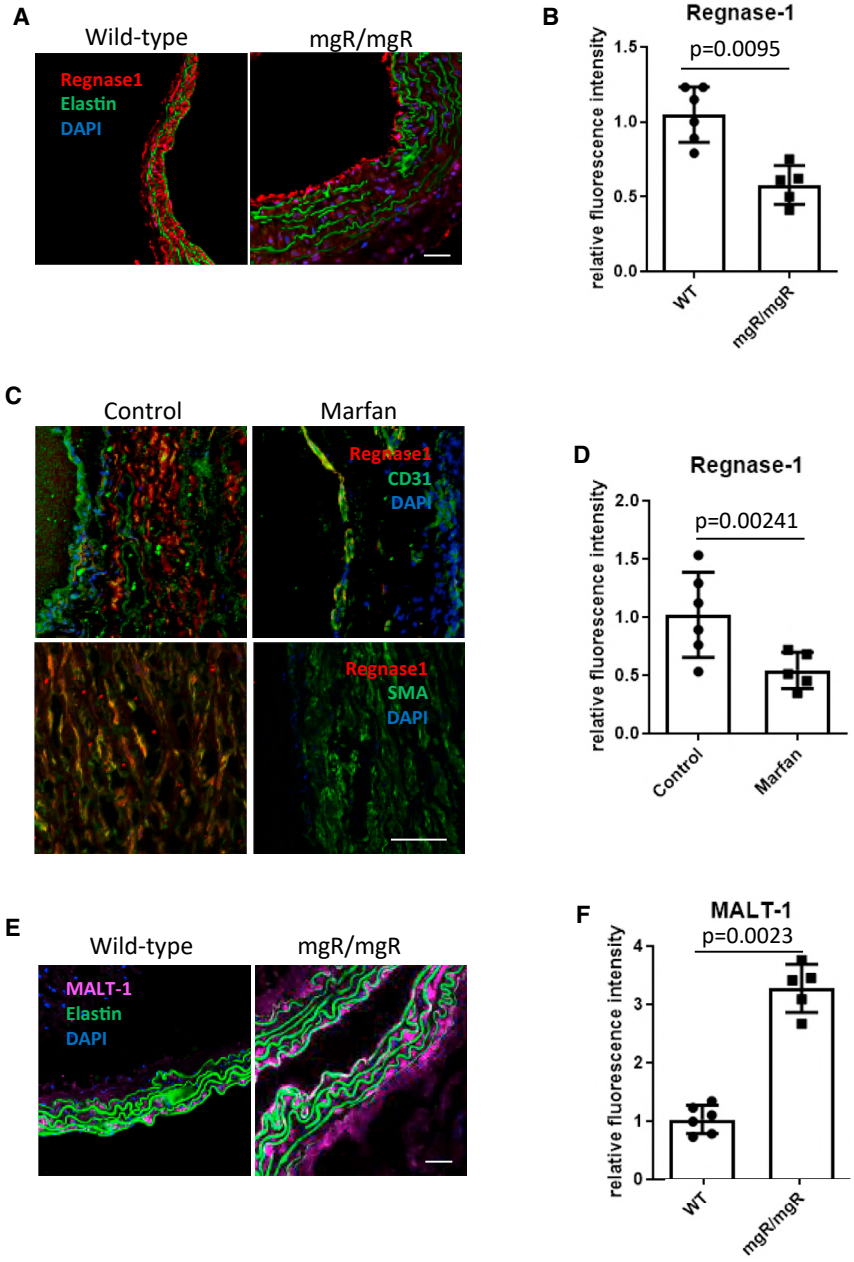


Figure 1. Decreased regnase-1 expression in aortic SMCs of mgR/mgR mice and Marfan patients

(A) Representative images showing regnase-1 expression in murine thoracic aortic tissue (red). Nuclei were stained with DAPI (blue), and the autofluorescence of elastic fibers was visualized on the green channel. The scale bar represents 50 μm, and asterisks show the aortic lumen). (B) Statistical quantification of mean red fluorescence intensity in immunohistochemistry pictures (n = 5, 15 images analyzed/group). Asterisks show the aortic lumen. (C) Illustrative images showing regnase-1 expression in human thoracic aortic tissue from controls and Marfan patients. The scale bar represents 50 μm. (D) Statistical quantification of red mean fluorescence intensity in the media of human samples (n = 4, 16 images analyzed/group). (E) Illustrative immunohistochemistry image showing MALT-1 expression (magenta) in murine thoracic aortic cryosections. Elastin fluorescence was visualized on the green channel. DAPI (blue) was used to mark cell nuclei. Asterisks show the aortic lumen. (F) Corresponding quantification of mean fluorescence intensity as a marker for MALT-1 expression (n = 5, 15 images analyzed/group).

oxidative stress.[11] Interestingly, cytokines such as IL-1β, TGF-β, and lipopolysaccharides induce the expression of regnase-1.[12]

We hypothesized that regnase-1 has protective effects on the progression of aortic aneurysms due to its anti-inflammatory properties and possibly its influence on elastolysis in the media. In this study, we aimed to determine whether adeno-associated virus (AAV)–mediated regnase-1 overexpression leads to an improvement in vessel structure, a decrease in inflammatory parameters, and subsequently, to a reduction in aortic dilatation with respect to its potential as a novel gene therapy approach for Marfan syndrome.

RESULTS

Decreased regnase-1 expression in SMCs of mgR/mgR mice and Marfan patients as compared to controls

We aimed to determine whether regnase-1 expression is dysregulated in aortic sections of Marfan mice. As shown in Figures 1A and 1B, regnase-1 expression was significantly decreased in the media of mgR/mgR mice. To confirm these findings in human samples, we subjected aortic cryosections from Marfan patients and controls to immunohistochemistry. Our analyses confirmed a similar pattern as in murine samples, namely, reduction in regnase-1 endoribonuclease levels in the media of Marfan patients (Figures 1C and 1D). To further substantiate a molecular mechanism behind these observations, we assessed the expression pattern of MALT-1, a well-characterized protease cleaving regnase-1 in immune cells.[13] As depicted in Figures 1E and 1F, Marfan aortic sections of mice showed a significant increase in MALT-1 protein level compared to corresponding controls.

Regnase-1 overexpression in mouse SMCs decreases IFN-γ-induced proinflammatory environment

We further aimed to substantiate the effect of regnase-1 overexpression in SMCs, regarding a proinflammatory environment *in vitro*. Transgene overexpression was achieved using endothelial-targeted AAV9SLR, showing efficient vascular cell transduction efficiency *in vitro*.[14] As proven in Figures 2A and 2B, we achieved a 1.7-fold overexpression of regnase-1 following AAV9SLR transduction in

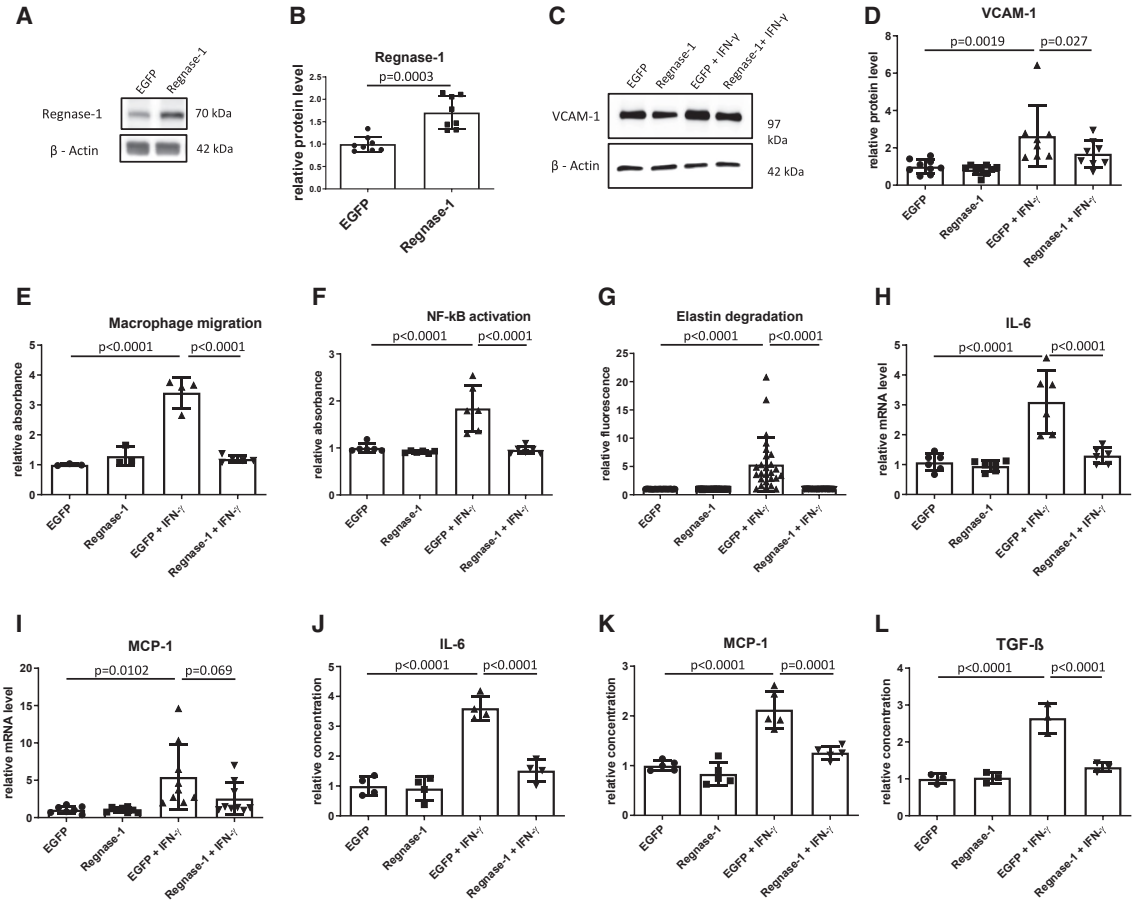


Figure 2. Regnase-1 overexpression decreases proinflammatory markers and elastin degradation in mouse SMCs *in vitro*

(A) Illustrative images of western blots showing protein levels of regnase-1 and β-actin as loading control in cell lysates of murine SMCs following AAV9SLR transduction. (B) Corresponding statistical quantification of regnase-1 levels in treated cells. Values were normalized to EGFP-treated SMCs (3 independent experiments). (C) Illustrative images of western blots showing protein levels of VCAM-1 and β-actin as loading control in cell lysates of murine SMCs in the depicted treatment groups. (D) Corresponding statistical quantification of VCAM-1 level. EGFP-transduced cells served as controls (3 independent experiments). (E) Degree of macrophage migration toward the supernatant of SMCs in the depicted treatment groups, indicating different levels of promigratory cytokines (3 independent experiments). (F) Assessment of NF-κB activation in murine SMC in different treatment groups (3 independent experiments). (G) Degree of elastin degradation in treated murine SMCs measured fluorometrically (3 independent experiments). (H and I) Statistical quantification of relative mRNA levels of proinflammatory cytokines IL-6 and MCP-1 in murine SMCs following transduction. GAPDH served as a housekeeping gene. EGFP-transduced cells were used as controls for normalizing gene expression (3 independent experiments). (J–L) Levels of secreted proinflammatory cytokines in the supernatant of SMC following transduction and proinflammatory stimulation, measured using ELISA (3 independent experiments).

our *in vitro* setup. Furthermore, as shown in Figures 2C and 2D, regnase-1 overexpression significantly decreased the level of vascular cell adhesion molecule 1 (VCAM-1) in the presence of interferon-γ (IFN-γ) as a proinflammatory cytokine. Next, we determined the ability of SMC-derived supernatants to induce macrophage migration *in vitro*. As expected, cells treated with control AAV-EGFP demonstrated the highest promigratory capacity under IFN-γ stimulation.

In contrast, supernatant isolated from AAV9SLR-regnase-1 transduced SMCs induced a lower degree of macrophage migration as controls (Figure 2E). Interestingly, our experiments point toward a significant reduction in nuclear factor κB (NF-κB) activation upon AAV9SLR-regnase-1 treatment in cultured SMCs as compared to control (Figure 2F). Because elastin degradation is a hallmark of Marfan syndrome,[15] we also investigated a potential impact of regnase-1 overexpression on this parameter. The results demonstrate that although IFN-γ induced a marked increase in elastin proteolysis in SMCs, this could be almost entirely abrogated by regnase-1 overexpression before cytokine stimulation (Figure 2G). In addition, several well-characterized regnase-1 targets were significantly decreased in both mRNA and protein levels following regnase-1 overexpression (Figures 2H–2L). More important, these results could be reproduced in human SMCs isolated from Marfan patients (Figure S1). All in all, these findings indicate that regnase-1 overexpression significantly affects the proinflammatory environment in SMCs.

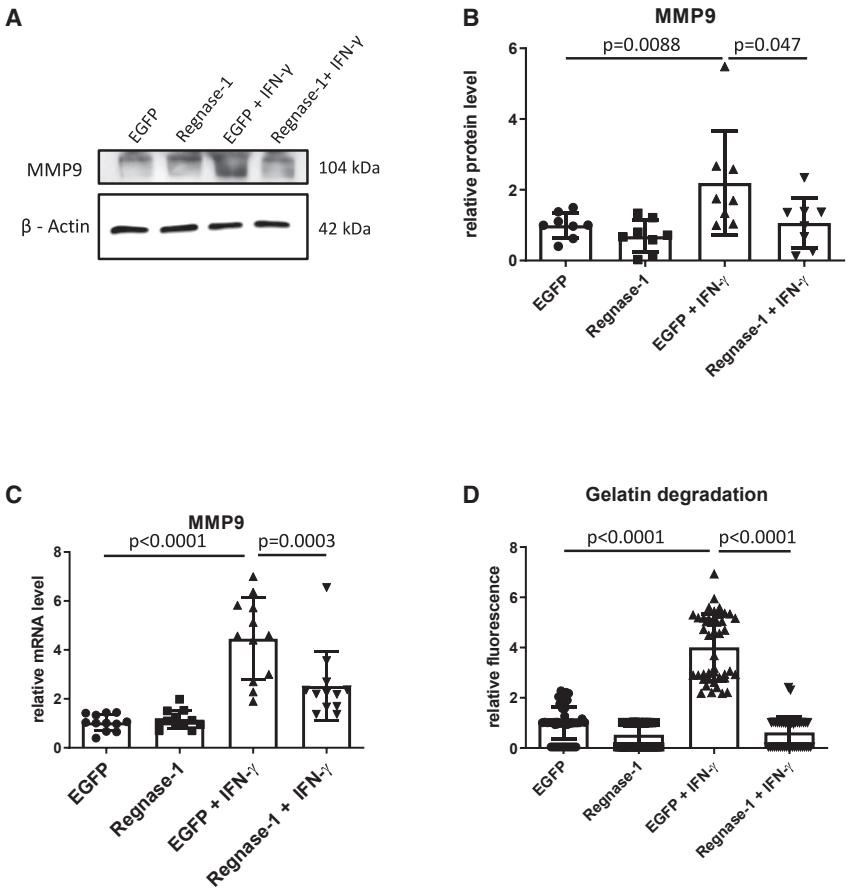


Figure 3. Regnase-1 overexpression decreases MMP9 expression and activity in mouse SMCs *in vitro*

(A) Illustrative images of western blots showing protein levels of MMP9 and β-actin, used as loading control in cell lysates of murine SMCs in different treatment groups. (B) Corresponding quantification of relative MMP9 protein levels following transduction (3 independent experiments). (C) Expression levels of MMP9 in murine SMCs in different treatment groups. GAPDH was used as a housekeeping gene (3 independent experiments). (D) Degree of gelatin degradation in murine SMCs in different treatment groups (3 independent experiments).

Regnase-1 overexpression decreases MMP9 expression and activity in SMCs *in vitro*

MMP9 activity directly contributes to aortic remodeling in the context of Marfan syndrome.[16] Hence, we next aimed to determine whether its expression is affected by the AAV-mediated upregulation of regnase-1 *in vitro*. Our data show that although MMP9 expression significantly increased upon IFN-γ stimulation, its levels markedly decreased following regnase-1 overexpression in both mRNA and protein levels (Figures 3A–3C). We could also detect a significant decrease in gelatinase (MMP2 and MMP9) activity in SMCs' supernatant, as proven in Figure 3D. These findings could be translated into human SMCs (Figure S2). Because regnase-1 was proven to induce apoptosis in cancer cells,[17] we assessed whether a toxic effect could be noted in our *in vitro* system. For this purpose, we subjected transduced SMCs to TUNEL and 3-[4,5-dimethylthiazole-2-yl]-2,5-diphenyltetrazolium bromide (MTT) assays. In contrast to tumor cells, regnase-1 overexpression did not diminish cell viability and did not induce apoptosis (Figure S3).

Successful vascular cell transduction following AAV9-G2^{CNN} injection

The aforementioned *in vitro* results prompted us to analyze the effect of regnase-1 overexpression in an *in vivo* setting. Thus, we injected 8-week-old Marfan mice with G2^{CNN}-tagged AAV9 expressing either regnase-1 or EGFP as a control (Figure 4A). Three out of 10 AAV-EGFP–injected mice and 2 out of 12 AAV-regnase-1–treated mice died early (11–12 weeks of age) during treatment, presumably due to aortic aneurysm dissection. As depicted in Figures 4B and 4C, tail vein injection led to successful transgene expression in endothelial cells and in the media and adventitia. In addition, this observation was confirmed by western blot analysis (Figures 4D and 4E). To confirm that regnase-1 was indeed overexpressed upon targeted AAV9 injection, we subjected cryosections to immunohistochemistry using a specific antibody. As shown in Figures 4F and 4G, we could achieve a significant 3-fold increase in regnase-1 expression following AAV9-regnase-1 injection as compared to control.

Regnase-1 overexpression in aortic vascular cells improves elastin architecture and decreases aortic size in Marfan mice

Next, we aimed to define the effect of regnase-1 overexpression in aortic cells in the well-established model of Marfan syndrome. Elastin van Gieson staining and subsequent quantification of the number of "islands of damage" revealed that although control EGFP-injected male Marfan mice presented with a highly fragmented aortic wall, regnase-1 overexpression markedly ameliorated this phenotype (Figures 5A and 5B). Coinciding with the decrease in the number of islands of damage in AAV-regnase-1 overexpressing mice, we could detect a significant reduction in aortic diameter, measured by echocardiography, pointing toward stabilization of the aortic wall following our gene therapy approach (Figures 5C–5E). The protective effect of regnase-1 overexpression on the development of elastin breaks and aortic dilatation could also be confirmed in female mice (Figure S4).

Regnase-1 overexpression in aortic vascular cells decreases proinflammatory markers in the aortic tissue of mgR/mgR mice

To gain deeper insights into the molecular players participating in the observed positive effect on the Marfan aortic wall, we measured the

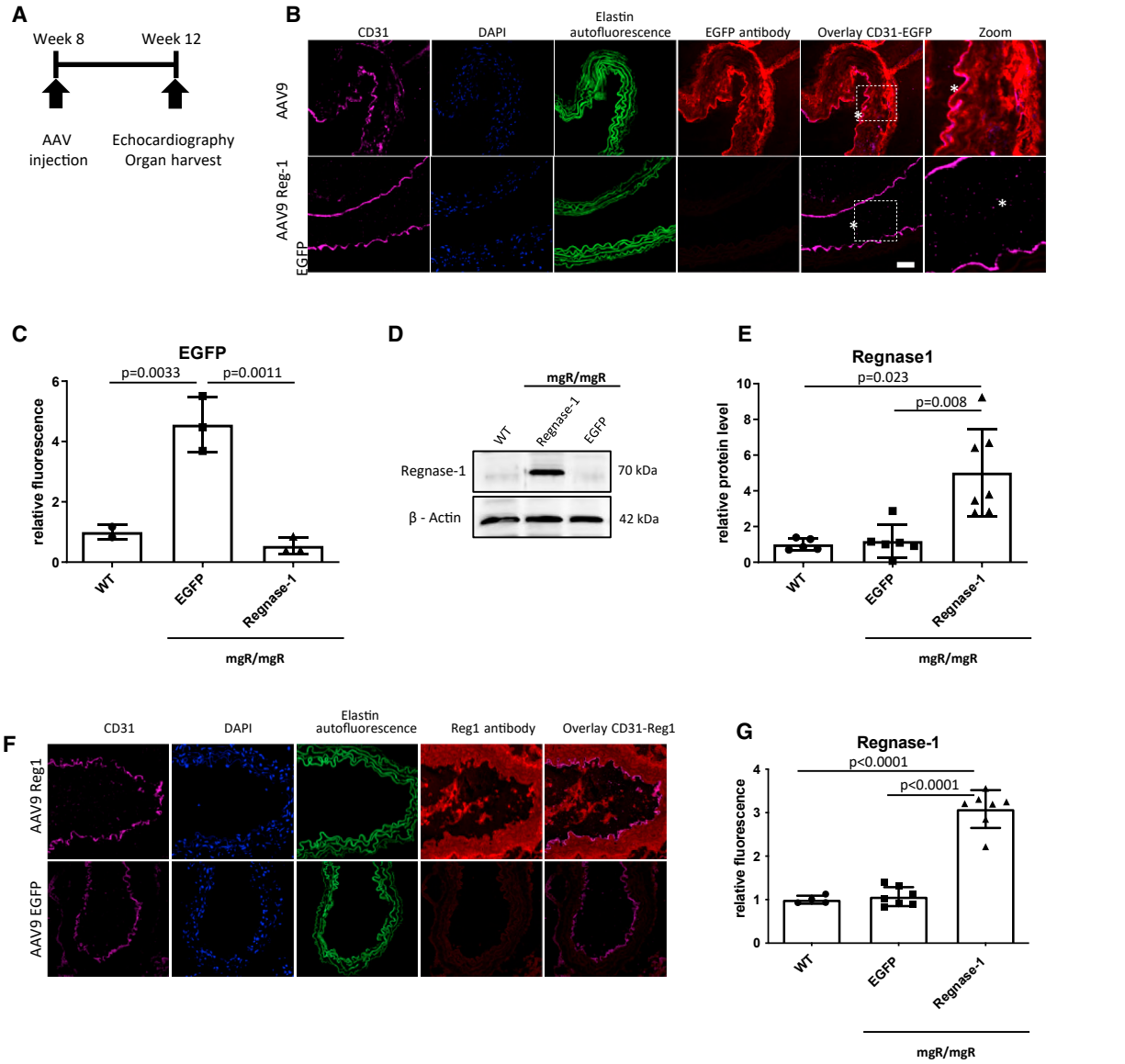


Figure 4. Targeted transgene overexpression following AAV injection in male mgR/mgR mice

(A) Schematic representation of the experimental design of the *in vivo* study. (B) Representative immunohistochemistry images showing EGFP expression in murine thoracic aortic tissue (red) for mice injected with AAV9-G2^{CNN}-EGFP (upper line) and AAV9-G2^{CNN}-regnase-1 (lower line). Boxed images show successful transduction of both endothelial and SMCs. Nuclei were stained with DAPI (blue). The autofluorescence of elastic fibers was visualized on the green channel. Asterisks show the aortic lumen. The scale bar represents 25 μm. (C) Statistical quantification of mean red fluorescence intensity showing EGFP levels within the aortic wall following injection of AAV9-G2^{CNN} (n = 3, 9 images analyzed/group). (D) Illustrative images of western blots showing protein levels of regnase-1 and β-actin as loading control in tissue lysates of murine aortas following transduction. Tissue isolated from WT mice served as control. (E) Corresponding statistical quantification of protein levels of regnase-1 in depicted treatment groups and WT mice (n = 5 for WT mice, n = 6 for AAV-EGFP injected mice, n = 7 for AAV-regnase-1 injected mice). (F) Illustrative images showing regnase-1 (Reg1) levels in aortic sections of mice in the depicted treatment groups (red). CD31 (magenta) was used to label endothelial cells, and elastin autofluorescence is shown in green. DAPI (blue) was used as a nuclear marker. (G) Statistical quantification of red mean fluorescence intensity, corresponding to regnase-1 protein levels in analyzed sections (n = 5 for WT mice, n = 6 for AAV-EGFP-injected mice, n = 7 for AAV-regnase-1-injected mice).

expression of MMP9 and proinflammatory markers following AAV transduction. As shown in Figures 6A and 6B, regnase-1 overexpression led to a significant reduction in MMP9 protein levels, shown by immunohistochemistry. In addition, we could observe a marked decrease in MMP2 and elastase MMP12 mRNA levels in the aortic tissue of mice injected with AAV-regnase1 as compared to control mgR/mgR mice (Figure S5). Likewise, staining with VCAM-1 and MCP-1 antibodies demonstrated a similar pattern: a marked decrease

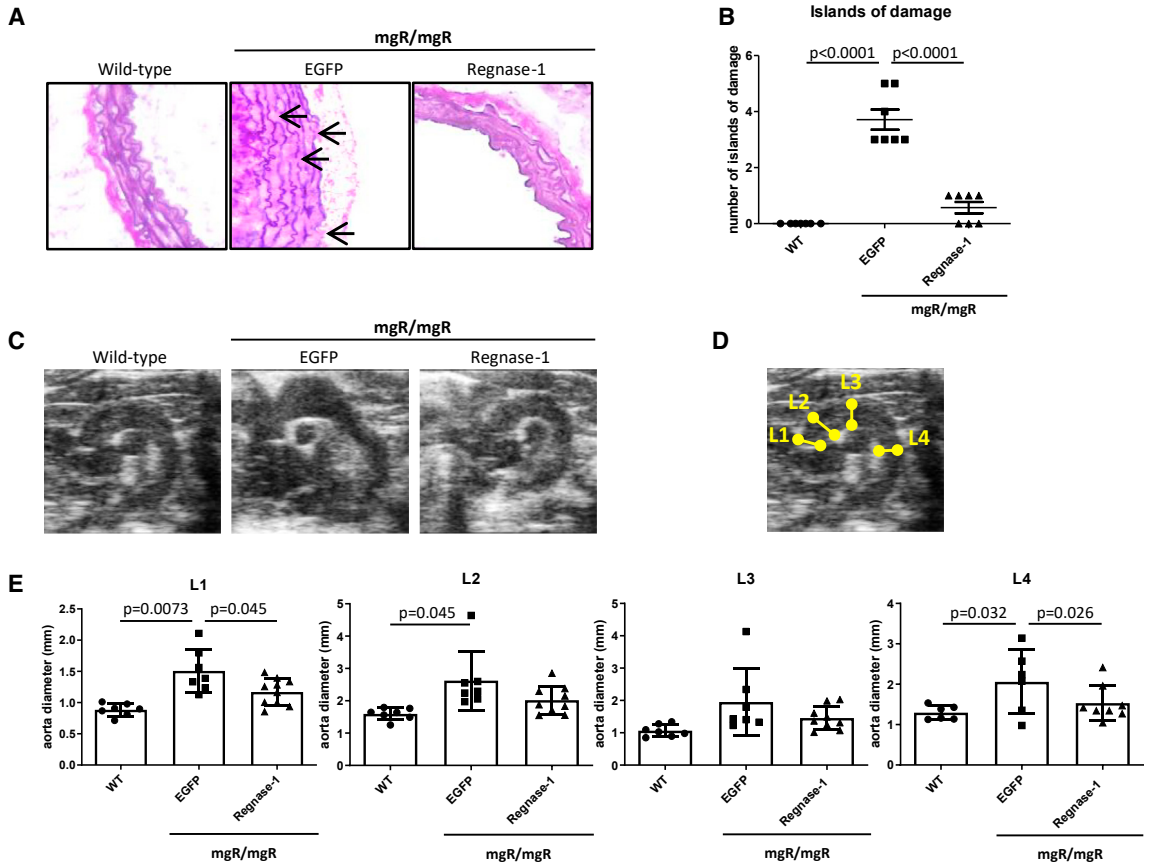


Figure 5. Regnase-1 overexpression improves elastin architecture and decreases aortic aneurysm size in male mgR/mgR mice

(A) Representative images of thoracic aortic cryosections subjected to elastic van Gieson staining. Elastic fibers appear black and collagen appears red. Arrows indicate islands of damage. The scale bar represents 25 μm. (B) Statistical quantification of the number of islands of damage in the media in different treatment groups of mgR/mgR mice and WT mice as controls (n = 7). (C) Representative echocardiographic images of the thoracic aorta for different treatment groups and WT mice used as controls. (D) Illustrative image showing areas where aortic size was measured in an ultrasound image. (E) Statistical quantification of aortic diameter at aortic annulus (L1), sinotubular junction (L2), aortic arch (L3), and proximal descending aorta (L4) in mice subjected to the designed gene therapy approach and WT mice (n = 7 for WT mice and AAV-EGFP-injected mice, n = 10 for AAV-regnase-1-injected mice).

in mice receiving the designed gene therapy approach (Figures 6C–6F). Similarly, we could detect a dramatic reduction in circulating levels of IL-6 and MCP-1 in the plasma of treated mice (Figures 6G and 6H). Because IL-6, MCP-1, and IL-12 are major cytokines influenced by regnase-1, we next measured their expression on mRNA level in aortic tissue. Indeed, there was a trend toward reducing mRNA levels of MCP-1 in the aortas of Marfan mice treated with AAV9-G2CNN-regnase1 compared to controls, whereas the expression levels of IL-6 and IL-12 were significantly decreased by our treatment (Figure 6I–6K).

DISCUSSION

Here, we show that targeting proinflammatory responses by overexpressing endoribonuclease regnase-1 in the aortic tissue of Marfan mice can halt the progression of thoracic aortic aneurysms by decreasing key cytokines involved in disease progression. Notably, mice receiving our gene therapy approach presented with improved elastin architecture in thoracic aortic tissue, decreased MMP expression, and reduced circulating levels of IL-6 and TGF-β. Because the leading cause of mortality in Marfan mice and patients is thoracic aortic aneurysm dissection, we focused mainly on this aortic region for molecular and histological analyses.[18]

A well-established hallmark of aortic aneurysm dissection associated with Marfan syndrome is developing a proinflammatory environment.[7] Marfan patients exhibit increased amounts of circulating cytokines and enhanced infiltration of inflammatory cells in the adventitia and media.[7] Similarly, Marfan mice present with infiltration of proinflammatory leukocytes in early age.[19] Proinflammatory cells produce MMPs able to digest elastin and extracellular matrix components. In turn, degradation products act as chemotaxis agents for macrophages, promoting further inflammatory cascades and disease progression.[20,21]

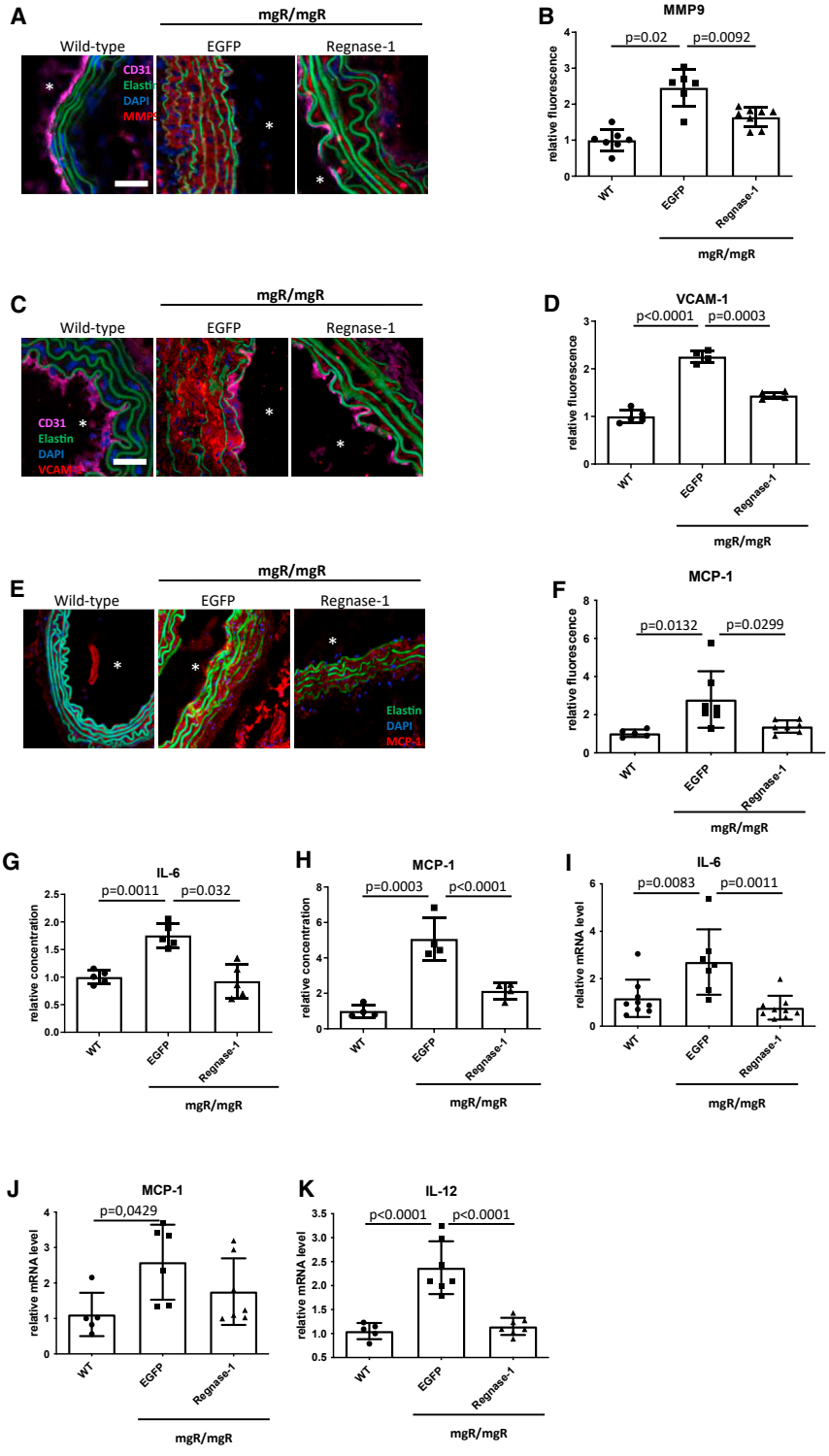


Figure 6. Aortic regnase-1 overexpression decreases MMP expression and inflammation in male mgR/mgR mice

(A) Representative images showing MMP9 expression in murine thoracic aortic tissue (red) for the depicted treatment groups and WT mice. Nuclei were stained with DAPI (blue). The autofluorescence of elastic fibers was visualized on the green channel. Asterisks show the aortic lumen. The scale bar represents 50 μm. (B) Statistical quantification of mean red fluorescence intensity in immunohistochemical analyses as a measure of MMP9 expression in the aortic wall of different treatment groups and WT mice (n = 7 for WT mice, n = 6 for AAV-EGFP-injected mice, n = 8 for AAV-regnase-1-injected mice, 3 images/section. (C) Illustrative images showing VCAM-1 expression (red) in thoracic aortic sections from mice in the depicted groups. DAPI (blue) was used as a nuclear counterstaining, and elastin autofluorescence is shown in green. The scale bar represents 50 μm, and asterisks depict the aortic lumen. (D) Statistical quantification of VCAM-1 protein level in thoracic aortic tissue. WT mice served as controls (n = 5 for WT mice and AAV-regnase-1-injected mice, n = 4 for AAV-EGFP-injected mice, 3 images/section. (E and F) Representative images (E) showing MCP-1 staining (red) of aortic tissue in frozen sections of mice subjected to the underlined treatment groups and (F) statistical quantification of fluorescence intensity as a measure of MCP-1 levels in analyzed tissues. (G and H) Statistical quantification of serum levels of IL-6 and MCP-1 in treated mice, measured by ELISA. WT mice served as controls (n = 5). (I–K) Statistical quantification of relative mRNA levels of proinflammatory cytokines IL-6, MCP-1, and IL-12 in aortas of treated and WT mice. GAPDH was used as a housekeeping gene (n = 9 for WT mice, n = 7 for AAV-EGFP-injected mice, n = 8 for AAV-regnase-1-injected mice).

Although regnase-1 expression was first characterized in immune cells,[9] the endoribonuclease was subsequently detected in epithelial cells, where it acts as a proinflammatory player and maintains epithelial layer integrity.[10] Interestingly, endothelial cell-specific regnase-1 deletion induces proinflammatory and prothrombotic factors, further progressing to endothelial permeability and vascular dysfunction.[22] In consistency, the absence of regnase-1 causes exacerbated neuroinflammation and increased infarction size.[23] Likewise, our results delineate a broader role of regnase-1 in the vasculature, particularly in maintaining the homeostasis of SMCs under inflammatory insult, decreasing the expression of MMPs, and decreasing the degree of circulating proinflammatory cytokines in the context of aortic aneurysms associated with Marfan syndrome.

Cytokine mRNA levels are tightly controlled transcriptionally. Regnase-1 suppresses an abnormal proinflammatory environment by recognizing and degrading specific secondary RNA structures.[9]

Interestingly, our results demonstrate decreased regnase-1 expression in the media of Marfan mice, which could account for exacerbated inflammation and increased MMP expression in this model. This is contradictory to increased circulating TGF-β levels as a hallmark of Marfan patients.[24] However, TGF-β triggers the activation of mucosa-associated lymphoid tissue lymphoma translocation protein 1 (MALT-1) paracaspase and NF-κB pathway in cancer cells.[25] Consistently, our findings prove increased MALT-1 expression in the SMCs of Marfan mice, providing mechanistic support for reduced endoribonuclease expression within the aortic wall. MALT-1 was demonstrated to induce the cleavage of regnase-1 in immune cells as a critical step for controlling T cell activation.[13] Moreover, MALT-1 was shown to be a major player in Ang II-induced vascular inflammation in the context of aortic aneurysm by activating the NF-κB pathway.[26] Therefore, we hypothesize that although TGF-β drives the expression of regnase-1 in Marfan syndrome, these increases in protein levels of the endoribonuclease are blunted by increased MALT-1 expression and activity.

The most prominent finding of our study is a dramatic decrease in circulating IL-6 levels following tail vein administration of regnase-1 overexpressing AAV. Enhanced IL-6 signaling regulated aortic dilatation and aneurysm formation in Marfan mice.[8] In addition, we could prove the reduced expression of vascular adhesion protein VCAM-1 *in vitro* and *in vivo*. These observations are in agreement with previous reports showing that regnase-1 overexpression can markedly decrease the expression of VCAM-1 in endothelial cells under pro-inflammatory conditions.[27] Conversely, increasing regnase-1 expression by applying MALT-1 inhibitor significantly suppressed the expression of VCAM-1 and intercellular adhesion molecule 1 in cultured endothelial cells.[28]

Our data show decreased TGF-β levels following regnase-1 overexpression. Although TGF-β was initially thought to be the main contributor of aortic dissections associated with Marfan syndrome,[24,29] others reveal controversial findings.[30,31] Abnormal TGF-β signaling was proven in thoracic aortic tissue on the single-cell level.[32] In addition, TGF-β was demonstrated to contribute to the senescence of SMCs in aortic aneurysms.[33] One possible explanation could be based on the different ages and strains of Marfan mice used in various experimental settings. These findings are of major significance and highlight the importance of choosing the right timing for an anti-inflammatory therapy for Marfan syndrome.

One crucial observation is that treatment with regnase-1 overexpressing AAV did neither induce apoptosis nor decrease cell viability in our *in vitro* and *in vivo* setup. Regnase-1 upregulation in cancer cells led to enhanced caspase activity and the induction of apoptotic processes.[34] However, regnase-1 is also known as a regulator of cancer cell proliferation *in vivo*.[35] These contradictory findings could be related to a different micro RNA signature in SMCs compared to cancer cells.

The main limitation of our study is the lack of a long-term study to evaluate whether the proposed therapy approach can prolong the survival rate of Marfan mice. These experiments would be precious before clinical translation. In addition, we injected the therapeutic AAVs at 8 weeks of age, when mice are generally not yet affected by aneurysm dissection, but aortic elastin architecture is already disturbed, which could account for similar mortality rates between the two experimental groups. Marfan mice could be treated at various time points, corresponding to several degrees of aneurysm severity, to determine the most effective approach for therapy. An earlier time point could lead to a more dramatic improvement in the pathological changes associated with the disease. Moreover, although the mouse model for Marfan syndrome recapitulates the main pathological features of the disease, a large animal model is more compatible with the patient's situation and can bring more insights into the translational perspectives of our study.[36] Finally, a concise investigation of macrophage infiltration would be interesting in subsequent studies.

In conclusion, our data underline a novel therapeutic approach for limiting the development of aortic aneurysms in Marfan syndrome. Furthermore, for the first time, we prove that the overexpression of therapeutic genes in the aortic wall is highly effective using a coating approach, as previously described.[37] Last but not least, our study provides evidence for the intense contribution of abnormal proinflammatory cascades in aortic aneurysm progression in Marfan syndrome.

MATERIALS AND METHODS

Mouse model

All of the animal experiments were carried out according to the institutional rules and in agreement with animal welfare protocols in Schleswig-Holstein (permission no. V242-55381/2019). Mice were kept at 23°C in 10-h/14-h light/dark cycles, with *ad libitum* feeding. AAV9 vectors harboring either EGFP or regnase-1 were coated with nanoparticles, as previously described, and systemically injected through tail vein injection into 8-week-old male and female Marfan mgR/mgR mice.[37] Each mouse was injected with 10^{12} genomic particles AAV in a total volume of 100 μL. Four weeks after the injection, thoracic aorta and blood samples were analyzed. Gender-matched and age-matched wild-type (WT) mice served as controls. Mice were sacrificed by cervical dislocation.

Human samples

Aortic tissue was obtained from Marfan patients and healthy controls undergoing surgical treatment following written consent under ethics vote at the University Clinic Schleswig-Holstein Kiel (permission no. D495/19 by the Ethics Committee of the University Medical Centre Schleswig-Holstein, Kiel) and University Clinic Heidelberg (S-260/2021 by the Ethics Committee at the Faculty of Medicine, University of Heidelberg). Four male patients (ages 31–59 years) were included in our study. Only thoracic aneurysmal tissue was further processed for SMC isolation.

Ultrasound-based assessment of aortic diameters

To determine aortic diameters, we used a Vevo 1100 ultrasound system (VisualSonics, Fujifilm Sonosite B.V.) equipped with an MS400 transducer and a central frequency of 30 MHz and a focal length of 7.0 mm. Anesthesia was induced by putting the mouse in an induction chamber using 3% isoflurane and 1 L/min 100% oxygen for 1–2 min, followed by inhalation anesthesia with 1.5–2% isoflurane using a mask around the nose.[38] Electrocardiogram electrodes and a rectal probe measured heart rate and body temperature. The aortic diameters (aortic annulus [L1], sinotubular junctions [L2], aortic arch [L3], and proximal descending aorta [L4]) were measured from the B mode aortic arch view, as previously described.[39] The diameter of these aortic regions was already proven to be highly increased in Marfan mice.[39]

Isolation, culture, and treatment of primary SMCs

Murine primary aortic SMCs were isolated from the aortas of mgR/mgR mice, as previously described.[40] Cells were cultured in a complete DMEM medium supplemented with 15% fetal bovine serum, 50 U/mL penicillin, 50 μg/mL streptomycin, and 2 mmol/L L-glutamine (Thermo Fisher Scientific). Cells cultured up to passage 4 were used in all of the experiments. SMCs were plated on plastic cell culture dishes (Thermo Fisher Scientific) or gelatin-coated glass coverslips when used for imaging experiments. Transduction with either AAV9SLR-EGFP or AAV9SLR-regnase-1 in a serum-free medium was performed when cells reached 80% confluency. At 48 h after transduction, inflammation was induced by treatment with 100 ng/mL IFN-γ for 24 h for protein analysis and gene expression evaluation. The supernatant was collected and kept at −80°C until further analysis.

AAV production

AAV9 (for *in vivo* studies) and AAV9SLR (for *in vitro* studies) expressing either regnase-1 or EGFP under the regulation of cytomegalovirus promoter were produced and further purified, as previously described.[14,41] Endothelial targeting of AAV9 for *in vivo* experiments was achieved by coating with endothelial-affine peptide, as described before.[37] In brief, complexes of AAV9 and coating particle $G2^{CNN}$ were formed by incubation in Opti-MEM medium for 30 min at room temperature before injection into mice.

qRT-PCR

According to the manufacturer's instructions, the total RNA was isolated from SMC and aortic tissue using the RNeasy kit (Qiagen). cDNA synthesis was accomplished using LunaScript RT SuperMix Kit (New England Biolabs) starting from 1 μg RNA. qRT-PCR was performed using SYBR Green (Qiagen) and specific primers for the genes of interest (Table S1). Gene expression was normalized to glyceraldehyde 3-phosphate dehydrogenase (GAPDH).

Western blot analysis

Protein samples from cells and tissue were isolated using radioimmunoprecipitation assay lysis buffer supplemented with protease inhibitors and were then electrophoresed in 10% SDS-PAGE and blotted onto nitrocellulose or polyvinylidene fluoride membrane. Nonspecific binding was blocked by incubation for 1 h in 5% BSA (Merck) or 5% nonfat dry milk (Roth) diluted in Tris-buffered saline with 0.1% Tween 20 detergent buffer. The dilutions of the primary antibodies used in our study are as follows: regnase-1 (Invitrogen, PA5-22137, 1:1,000), MMP9 (Abcam, ab38898, 1:1,000), VCAM1 antibody (Abcam, ab134047, 1:1,000), β-actin (Sigma-Aldrich, A5441, 1:20,000), and GAPDH (Sigma-Aldrich, G8795, 1:20,000). β-Actin and GAPDH served as internal controls, proving equal loading of the protein samples. Corresponding horseradish-coupled secondary antibodies (anti-rabbit-horseradish peroxidase [HRP] and anti-mouse-HRP) were obtained by Dianova, and imaging was performed with the ImageQuant LAS 4000 mini system (GE Healthcare Life Sciences).

NF-κB activation assay

First, nuclear extracts were isolated according to previously published protocols.[42] Second, samples were further processed according to the manufacturer's (Abcam) instructions. Equal amounts of protein were loaded in each well.

Macrophage transmigration assay

Transmigration assay was performed according to the manufacturer's (Biocat) Instructions. Supernatant from SMC cultured and treated as mentioned above was put in the lower chambers of a 24-well plate. The RAW cell suspension was placed in the transwell with an 8-μm polycarbonate membrane. During the incubation time of 24 h, cells were allowed to migrate through the membrane, depending on the amount of promigratory cytokines in the supernatant. Nonmigratory cells were removed, and migratory cells were dissociated from the membrane and lysed with the supernatant in the lower chamber. Fluorescent cell labeling dye provided in the kit was added for quantification, and fluorescence was measured (excitation/emission: 480 nm/520 nm) using the Cytation5 Imaging Reader (Biotek).

Staining of elastic fibers

Explants of thoracic aortae of mice were embedded in Tissue-Tek (Weckert Labortechnik) and cut into 7-μm-thick slices with a Cryostat (Microm HM 500 O). Elastin van Giesson stainings were performed according to the manufacturer's instructions (Sigma-Aldrich), and bright-field microscopy images were captured (Keyence). A blinded observer then counted the number of islands of damage per cross-section for each mouse, as previously described,[40] to assess the degree of elastin fragmentation in the media. An island of damage was defined as an area covering two fragmented elastic fibers, interposed with abnormal connective tissue deposition. Three aortic sections were analyzed per mouse.

Immunohistochemistry

Cryosections of aortic grafts 7 μm thick were fixed with 4% paraformaldehyde and then stained with the following primary antibodies: CD31 (Santa Cruz, sc-181916, 1:200) as an endothelial cell marker, regnase-1 (Thermo Fisher Scientific, PA5-22137, 1:300), MMP9 (Abcam, ab38898, 1:300), MALT-1 (Thermo Fisher Scientific, 39395,

1:400), MCP-1 (Abcam, ab25124, 1:300), and GFP (Thermo Fisher Scientific, A-31851, 1:400). Corresponding secondary antibodies were purchased from Invitrogen and used to a dilution of 1:300.

TUNEL assay

A TUNEL kit (Biomol) was used to determine the degree of DNA fragmentation in aortic tissue and cultured cells. Afterward, thoracic aortic sections or cells were stained with DAPI to mark cell nuclei. Imaging was performed using confocal microscopy. For *in vitro* experiments, H_2O_2-treated cells were used as a positive control, and DNase-treated aortic sections served as positive controls for *in vivo* settings.

MTT assay

Cell viability and proliferation was determined by using the MTT assay (Promega) according to standard protocols. In brief, transduced cells were incubated with MTT compound to a concentration of 0.2 mg/mL for 4 h. Next, cells were treated with a solubilization reagent and incubated overnight at 37°C. Next, absorption (570 nm) was measured using a Cytation 5 reader (BioTek).

Gelatin and elastin degradation assay

SMCs were treated with 40 ng/mL DQ-gelatin (Thermo Fisher Scientific) or elastin-fluorescein isothiocyanate (Anaspec) in a 96-well plate with black walls and transparent bottom (Greiner). Then, the mixture was incubated at 37°C for 2 h. Next, green fluorescence was measured using Cytation 5 reader (BioTek) as a measure of respective substrate degradation.

ELISA

ELISA was performed according to the manufacturer's (Biolegend) instruction to detect IL-6, MCP-1, and TGF-β levels. The supernatant of SMCs and plasma of mice served as samples. For the collection of plasma, blood was centrifuged at 1,500 × *g* for 10 min at 4°C before storage at −80°C. Plasma samples were diluted 1:3 before measurement.

Statistical analysis

In vitro experiments were performed in biological replicates mentioned in the corresponding figure legends. Three technical replicates were performed for each biologically different sample. Mice were matched for age and sex, and experimenters were blinded in the cases of ultrasound image analysis and counting of islands of damage. As indicated in figure legends, statistical analysis was performed using GraphPad Prism version 8. Before performing statistical analysis, datasets were tested for normal distribution (D'Agostino-Pearson test). The Mann-Whitney *U* test was performed to compare two experimental groups, and three or more sets were analyzed using one-way ANOVA followed by the Newman-Keuls posttest. $p < 0.05$ was considered significant. Exact p values are indicated on the graphs.

DATA AND CODE AVAILABILITY

The data that support the findings of this study are available from the corresponding authors A.R. and O.J.M. upon reasonable request.

SUPPLEMENTAL INFORMATION

Supplemental information can be found online at https://doi.org/10.1016/j.omtm.2023.101163.

ACKNOWLEDGMENTS

This project received funding from the European Union's Horizon 2020 research and innovation program under grant agreement no. 825670 (to O.J.M.) and the German Centre for Cardiovascular Research (DZHK) (81Z0700206, to O.J.M.).

AUTHOR CONTRIBUTIONS

A.R., A.H.W., D.F., N.F., and O.J.M. conceived the project. M.N., N.S., A.M., D.I.B., P.M.V.S., and A.R. performed the experiments under the supervision of A.H.W., C.K., D.F., N.F., A.R., and O.J.M. S.H. produced the AAVs. T.B. and A.H.W. produced the AAV coating. M.Z. and A.H.W. bred and characterized the mgR/mgR mice. R.A., T.P., and G.L. provided human biomaterial. M.N., D.I.B., and A.R. performed the *in vitro* studies and carried out the histological analyses. N.S. and A.M. operated on and euthanized the mice. M.N., N.S., and A.R. analyzed the data. M.N., A.R., and O.J.M. wrote the manuscript, with input from all of the authors. All of the authors approved the final manuscript.

DECLARATION OF INTERESTS

T.B. and C.K. have previously filed a patent application on the polymer coating for the vascular targeting of AAVs. The other authors declare no competing interests.

REFERENCES

1. Robinson, P.N., Arteaga-Solis, E., Baldock, C., Collod-Béroud, G., Booms, P., De Paepe, A., Dietz, H.C., Guo, G., Handford, P.A., Judge, D.P., et al. (2006). The molecular genetics of Marfan syndrome and related disorders. J. Med. Genet. *43*, 769–787.

2. Keane, M.G., and Pyeritz, R.E. (2008). Medical management of Marfan syndrome. Circulation *117*, 2802–2813.

3. Matt, P., Schoenhoff, F., Habashi, J., Holm, T., Van Erp, C., Loch, D., Carlson, O.D., Griswold, B.F., Fu, Q., De Backer, J., et al. (2009). Circulating transforming growth factor-beta in Marfan syndrome. Circulation *120*, 526–532.

4. Vasic, N., Glumac, S., Pejic, S., Amidzic, L.J., Tadic Latinovic, L.J., Dozic, B., Hinic, S., and Maksimovic, Z. (2017). Expression of Matrix Metalloproteinases and Endogenous Inhibitors in Abdominal Aortic Aneurysm and Aortoiliac Occlusive Disease (Syndrome Leriche). Folia Biol. *63*, 209–216.

5. Chung, A.W.Y., Au Yeung, K., Sandor, G.G.S., Judge, D.P., Dietz, H.C., and van Breemen, C. (2007). Loss of elastic fiber integrity and reduction of vascular smooth muscle contraction resulting from the upregulated activities of matrix metalloproteinase-2 and -9 in the thoracic aortic aneurysm in Marfan syndrome. Circ. Res. *101*, 512–522.

6. Chung, A.W.Y., Yang, H.H.C., Radomski, M.W., and van Breemen, C. (2008). Long-term doxycycline is more effective than atenolol to prevent thoracic aortic aneurysm in marfan syndrome through the inhibition of matrix metalloproteinase-2 and -9. Circ. Res. *102*, e73–e85.

7. Radonic, T., de Witte, P., Groenink, M., de Waard, V., Lutter, R., van Eijk, M., Jansen, M., Timmermans, J., Kempers, M., Scholte, A.J., et al. (2012). Inflammation aggravates disease severity in Marfan syndrome patients. PLoS One *7*, e32963.

8. Ju, X., Ijaz, T., Sun, H., Lejeune, W., Vargas, G., Shilagard, T., Recinos, A., 3rd, Milewicz, D.M., Brasier, A.R., and Tilton, R.G. (2014). IL-6 regulates extracellular matrix remodeling associated with aortic dilation in a fibrillin-1 hypomorphic mgR/mgR mouse model of severe Marfan syndrome. J. Am. Heart Assoc. *3*, e000476.

9. Mao, R., Yang, R., Chen, X., Harhaj, E.W., Wang, X., and Fan, Y. (2017). Regnase-1, a rapid response ribonuclease regulating inflammation and stress responses. Cell. Mol. Immunol. *14*, 412–422.
10. Dobosz, E., Wilamowski, M., Lech, M., Bugara, B., Jura, J., Potempa, J., and Koziel, J. (2016). MCPIP-1, Alias Regnase-1, Controls Epithelial Inflammation by Posttranscriptional Regulation of IL-8 Production. J. Innate Immun. *8*, 564–578.
11. Ribeiro, A., Dobosz, E., Krill, M., Kohler, P., Wadowska, M., Steiger, S., Schmaderer, C., Koziel, J., and Lech, M. (2022). Macrophage-Specific MCPIP1/Regnase-1 Attenuates Kidney Ischemia-Reperfusion Injury by Shaping the Local Inflammatory Response and Tissue Regeneration. Cells *11*.
12. Liang, J., Wang, J., Azfer, A., Song, W., Tromp, G., Kolattukudy, P.E., and Fu, M. (2008). A novel CCCH-zinc finger protein family regulates proinflammatory activation of macrophages. J. Biol. Chem. *283*, 6337–6346.
13. Uehata, T., Iwasaki, H., Vandenbon, A., Matsushita, K., Hernandez-Cuellar, E., Kuniyoshi, K., Satoh, T., Mino, T., Suzuki, Y., Standley, D.M., et al. (2013). Malt1-induced cleavage of regnase-1 in CD4(+) helper T cells regulates immune activation. Cell *153*, 1036–1049.
14. Varadi, K., Michelfelder, S., Korff, T., Hecker, M., Trepel, M., Katus, H.A., Kleinschmidt, J.A., and Müller, O.J. (2012). Novel random peptide libraries displayed on AAV serotype 9 for selection of endothelial cell-directed gene transfer vectors. Gene Ther. *19*, 800–809.
15. López-Guimet, J., Andilla, J., Loza-Alvarez, P., and Egea, G. (2017). High-Resolution Morphological Approach to Analyse Elastic Laminae Injuries of the Ascending Aorta in a Murine Model of Marfan Syndrome. Sci. Rep. *7*, 1505.
16. Xiong, W., Knispel, R.A., Dietz, H.C., Ramirez, F., and Baxter, B.T. (2008). Doxycycline delays aneurysm rupture in a mouse model of Marfan syndrome. J. Vasc. Surg. *47*, 166–172. discussion 172; discussion 172.
17. Miekus, K., Kotlinowski, J., Lichawska-Cieslar, A., Rys, J., and Jura, J. (2019). Activity of MCPIP1 RNase in tumor associated processes. J. Exp. Clin. Cancer Res. *38*, 421.
18. Jiménez-Altayó, F., Siegert, A.M., Bonorino, F., Meirelles, T., Barberà, L., Dantas, A.P., Vila, E., and Egea, G. (2017). Differences in the Thoracic Aorta by Region and Sex in a Murine Model of Marfan Syndrome. Front. Physiol. *8*, 933.
19. Pereira, L., Lee, S.Y., Gayraud, B., Andrikopoulos, K., Shapiro, S.D., Bunton, T., Biery, N.J., Dietz, H.C., Sakai, L.Y., and Ramirez, F. (1999). Pathogenetic sequence for aneurysm revealed in mice underexpressing fibrillin-1. Proc. Natl. Acad. Sci. USA *96*, 3819–3823.
20. Guo, G., Booms, P., Halushka, M., Dietz, H.C., Ney, A., Stricker, S., Hecht, J., Mundlos, S., and Robinson, P.N. (2006). Induction of macrophage chemotaxis by aortic extracts of the mgR Marfan mouse model and a GxxPG-containing fibrillin-1 fragment. Circulation *114*, 1855–1862.
21. Guo, G., Gehle, P., Doelken, S., Martin-Ventura, J.L., von Kodolitsch, Y., Hetzer, R., and Robinson, P.N. (2011). Induction of macrophage chemotaxis by aortic extracts from patients with Marfan syndrome is related to elastin binding protein. PLoS One *6*, e20138.
22. Jin, Z., Niu, J., Kapoor, N., Liang, J., Becerra, E., and Kolattukudy, P.E. (2019). Essential Role of Endothelial MCPIP in Vascular Integrity and Post-Ischemic Remodeling. Int. J. Mol. Sci. *20*, 172.
23. Liang, J., Wang, J., Saad, Y., Warble, L., Becerra, E., and Kolattukudy, P.E. (2011). Participation of MCP-induced protein 1 in lipopolysaccharide preconditioning-induced ischemic stroke tolerance by regulating the expression of proinflammatory cytokines. J. Neuroinflammation *8*, 182.
24. Neptune, E.R., Frischmeyer, P.A., Arking, D.E., Myers, L., Bunton, T.E., Gayraud, B., Ramirez, F., Sakai, L.Y., and Dietz, H.C. (2003). Dysregulation of TGF-beta activation contributes to pathogenesis in Marfan syndrome. Nat. Genet. *33*, 407–411.
25. Mazi, F.A., Cakiroglu, E., Uysal, M., Kalyoncu, M., Demirci, D., Sozeri, P.Y.G., Yilmaz, G.O., Ozhan, S.E., and Senturk, S. (2023). The paracaspase MALT1 is a downstream target of Smad3 and potentiates the crosstalk between TGF-beta and NF-kB signaling pathways in cancer cells. Cell. Signal. *105*, 110611.
26. McAllister-Lucas, L.M., Jin, X., Gu, S., Siu, K., McDonnell, S., Ruland, J., Delekta, P.C., Van Beek, M., and Lucas, P.C. (2010). The CARMA3-Bcl10-MALT1 signalosome promotes angiotensin II-dependent vascular inflammation and atherogenesis. J. Biol. Chem. *285*, 25880–25884.
27. Qi, Y., Liang, J., She, Z.G., Cai, Y., Wang, J., Lei, T., Stallcup, W.B., and Fu, M. (2010). MCP-induced protein 1 suppresses TNFalpha-induced VCAM-1 expression in human endothelial cells. FEBS Lett. *584*, 3065–3072.
28. Li, Y., Huang, S., Huang, X., Li, X., Falcon, A., Soutar, A., Bornancin, F., Jiang, Z., Xin, H.B., and Fu, M. (2018). Pharmacological inhibition of MALT1 protease activity suppresses endothelial activation via enhancing MCPIP1 expression. Cell. Signal. *50*, 1–8.
29. Benke, K., Ágg, B., Szilveszter, B., Tarr, F., Nagy, Z.B., Pólos, M., Daróczi, L., Merkely, B., and Szabolcs, Z. (2013). The role of transforming growth factor-beta in Marfan syndrome. Cardiol. J. *20*, 227–234.
30. Wei, H., Hu, J.H., Angelov, S.N., Fox, K., Yan, J., Enstrom, R., Smith, A., and Dichek, D.A. (2017). Aortopathy in a Mouse Model of Marfan Syndrome Is Not Mediated by Altered Transforming Growth Factor beta Signaling. J. Am. Heart Assoc. *6*, e004968.
31. Cook, J.R., Clayton, N.P., Carta, L., Galatioto, J., Chiu, E., Smaldone, S., Nelson, C.A., Cheng, S.H., Wentworth, B.M., and Ramirez, F. (2015). Dimorphic effects of transforming growth factor-beta signaling during aortic aneurysm progression in mice suggest a combinatorial therapy for Marfan syndrome. Arterioscler. Thromb. Vasc. Biol. *35*, 911–917.
32. Dawson, A., Li, Y., Li, Y., Ren, P., Vasquez, H.G., Zhang, C., Rebello, K.R., Ageedi, W., Azares, A.R., Mattar, A.B., et al. (2021). Single-Cell Analysis of Aneurysmal Aortic Tissue in Patients with Marfan Syndrome Reveals Dysfunctional TGF-beta Signaling. Genes *13*, 95.
33. You, W., Hong, Y., He, H., Huang, X., Tao, W., Liang, X., Zhang, Y., and Li, X. (2019). TGF-beta mediates aortic smooth muscle cell senescence in Marfan syndrome. Aging (Albany NY) *11*, 3574–3584.
34. Ligeza, J., Marona, P., Gach, N., Lipert, B., Miekus, K., Wilk, W., Jaszczynski, J., Stelmach, A., Loboda, A., Dulak, J., et al. (2017). MCPIP1 contributes to clear cell renal cell carcinomas development. Angiogenesis *20*, 325–340.
35. Marona, P., Górka, J., Mazurek, Z., Wilk, W., Rys, J., Majka, M., Jura, J., and Miekus, K. (2017). MCPIP1 Downregulation in Clear Cell Renal Cell Carcinoma Promotes Vascularization and Metastatic Progression. Cancer Res. *77*, 4905–4920.
36. Umeyama, K., Watanabe, K., Watanabe, M., Horiuchi, K., Nakano, K., Kitashiro, M., Matsunari, H., Kimura, T., Arima, Y., Sampetrean, O., et al. (2016). Generation of heterozygous fibrillin-1 mutant cloned pigs from genome-edited foetal fibroblasts. Sci. Rep. *6*, 24413.
37. Bozoglu, T., Lee, S., Ziegler, T., Jurisch, V., Maas, S., Baehr, A., Hinkel, R., Hoenig, A., Hariharan, A., Kim, C.I., et al. (2022). Endothelial Retargeting of AAV9 In Vivo. Adv. Sci. *9*, e2103867.
38. Tae, H.J., Petrashevskaya, N., Marshall, S., Krawczyk, M., and Talan, M. (2016). Cardiac remodeling in the mouse model of Marfan syndrome develops into two distinctive phenotypes. Am. J. Physiol. Heart Circ. Physiol. *310*, H290–H299.
39. Lee, L., Cui, J.Z., Cua, M., Esfandiarei, M., Sheng, X., Chui, W.A., Xu, M.H., Sarunic, M.V., Beg, M.F., van Breemen, C., et al. (2016). Aortic and Cardiac Structure and Function Using High-Resolution Echocardiography and Optical Coherence Tomography in a Mouse Model of Marfan Syndrome. PLoS One *11*, e0164778.
40. Arif, R., Zaradzki, M., Remes, A., Seppelt, P., Kunze, R., Schröder, H., Schwill, S., Ensminger, S.M., Robinson, P.N., Karck, M., et al. (2017). AP-1 Oligodeoxynucleotides Reduce Aortic Elastolysis in a Murine Model of Marfan Syndrome. Mol. Ther. Nucleic Acids *9*, 69–79.
41. Jungmann, A., Leuchs, B., Rommelaere, J., Katus, H.A., and Müller, O.J. (2017). Protocol for Efficient Generation and Characterization of Adeno-Associated Viral Vectors. Hum. Gene Ther. Methods *28*, 235–246.
42. Suzuki, K., Bose, P., Leong-Quong, R.Y., Fujita, D.J., and Riabowol, K. (2010). REAP: A two minute cell fractionation method. BMC Res. Notes *3*, 294.